Full Title:

Progressive engagement of SST+ interneurons via Elfn1 regulates the barrel-septa response identity in the somatosensory cortex of mice

Short Title:

Progressive engagement of SST+ neurons regulate barrel-septa identity

Authors:

Ali Özgür Argunşah[1,2], Tevye Jason Stachniak[1,2,3], Jenq-Wei Yang[1,2], Linbi Cai[1,2], George Kanatouris[1,2], Theofanis Karayannis[1,2,*]

[1]Laboratory of Neural Circuit Assembly, Brain Research Institute, University of Zurich Winterthurerstrasse 190, CH-8057 Zurich, Switzerland.

[2]Neuroscience Center Zurich, University of Zurich and ETH Zurich, Winterthurerstrasse 190, CH-8057 Zurich, Switzerland.

[3]Division of Biomedical Sciences, Faculty of Medicine, Memorial University of Newfoundland, St. John's, A1B 3V6, Canada.

[*]**Correspondence**: karayannis@hifo.uzh.ch

Abstract

The vibrissae system of rodents, akin to human hands and fingers, provides somatosensory information coming from individual whiskers for object exploration and recognition. Just as separated digits enhance somatosensation in humans, the ability of mice to sense objects through multiple whiskers in segregated streams is crucial. The segregation begins at the level of the whiskers and is maintained through their precise somatotopic organization in the Brainstem→ Thalamus→ Cortex axis, culminating in the so-called barrels and the in-between “spaces” called septa. Here, by performing *in-vivo*

silicon probe recordings simultaneously in the barrel and septa domains in mice upon repeated 10Hz single and multi-whisker stimulation, we identify and characterize a temporal divergence in the spiking activity between these domains. Further, through genetic fate-mapping, we reveal that cortical SST+ and VIP+ inhibitory neurons show a layer-dependent differential preference in septa versus barrel domains. Utilizing a genetic manipulation that affects the temporal facilitation dynamics onto only these two inhibitory cell classes, we largely abolish the temporal response divergence between the two cortical domains. Finally, using *in-vivo* viral tracing, whole-brain clearing and imaging, we show a differential barrel and septa projection pattern to cortical regions S2 and M1. We hence reveal that local temporally engaging cortical inhibition provided by SST+ neurons contribute to the functional segregation of barrel and septa domains and potentially their downstream targets.

Introduction

Although the somatosensory whisker system is one of the principal means by which mice sense their environment and navigate the world, the number of whiskers is relatively low. This relatively small number of vibrissae is represented in the whisker somatosensory cortex as barrel “islands” (columns) separated by the septal “sea” (compartments), reminiscent of the whisker pad pattern, with sparse hair follicles separated with significant spaces between them. In contrast, other sensory systems such as the auditory and the visual have densely packed anatomical receptor configurations and cortical representations. Although all sensory cortices are composed of canonical microcircuits[1] that include similar populations of excitatory and inhibitory neurons, maintaining separation of individual whisker information may require anatomical specializations found only in barrel cortex, such as the barrel and septa domains. These domains may therefore create a distinct spatiotemporal stimulus representation and information coding in the barrel cortex, compared to other sensory modalities.Such cortical columns have also been shown to exist in other sensory cortical areas organized in specific sensory-receptor to cortical-column mapping[2,3]. Cortical columns are thought to be separate processing units acting as transfer modules between converging sensory stimuli and cognitive faculties and/or motor output. In the barrel cortex, thalamocortical inputs coming from the

Ventro-Postero medial (VPM) and Postero-medial (PoM) nuclei segregate into the barrel and septa domains, respectively[4–7]. Further, information processing and flow within and from these domains target anatomically distinct sensory and motor areas[8–11]. It has been suggested that while the primary whisker somatosensory cortex (wS1) sends high dimensional information needed for object recognition to the secondary somatosensory cortex (wS2), the projections to the primary motor cortex (M1) carry less complex information unrelated to information coming from individual whiskers[6,10,12,13]. This divergence is also found in the barrel- and septa-related circuits. While barrel circuits are more involved in processing spatiotemporal whisker-object interactions, the septal circuits are more sensitive to the frequency of whisker movements, which suggests the use of temporal versus rate coding of information in barrel and septa, respectively[14,15]. Hence the existence of the septal region separating the barrels may provide the means that mice possess to separate these two interconnected yet very distinct information-processing routes along the temporal domain, in order to make sense of their somatosensory environment. This operational identity of barrels and septa has often been attributed to the parallel bottom-up thalamocortical pathways of the the VPM and PoM. Here, by performing *in-vivo* simultaneous silicon probe recordings in the barrel and septa domains in mice, we first characterize the temporal divergence between these domains. Through genetic labeling and passive tissue clearing, we reveal that cortical SST+ and VIP+ neurons show a layer-dependent differential distribution in the barrel versus septa domains. By altering the short-term synaptic dynamics of incoming excitation onto these interneurons upon removal of the synaptic protein *Elfn1*, we find that the domain-specific divergence of responses to a repetitive single-whisker stimulus is degraded. Finally, utilizing *in-vivo* retrograde viral-based tracing, we show a layer-specific projection preference between these domains and downstream regions wS2 and M1. Hence, in addition to the thalamocortical pathway-specific inputs, we reveal a key contribution of local lateral cortical inhibition provided by SST+ neurons in setting up the functional segregation of barrel and septa domains and subsequently the receiving downstream regions.

Results

Barrel and Septa columns display differentially adaptive spiking to repeated single whisker stimulation

To characterize the temporal stimulus response profiles of barrel and septal domains simultaneously, we performed *in-vivo* silicon probe recordings under urethane-induced light-anesthesia from mouse somatosensory whisker barrel cortex (wS1), after the onset age of whisking, postnatal day (P)20-30. Activity within identified barrels was recorded upon a 2s-long stimulation at 10Hz. Whisker stimulation was performed on either just one principal whisker (single-whisker stimulus or SWS, Figure 1A, 20 repetitions per principal whisker) or via both the principal whisker and most of the macro vibrissae together (multi-whisker stimulus or MWS, Supp. Figure 1A). Every mouse received both stimulation paradigms and post-hoc histology was used to assess the location of the multi-shank silicon probes, in order to assign the recorded activity to the stimulated principal barrel, the adjacent septa, or the adjacent unstimulated neighboring barrel (in the case of SWS) (Figure 1B and Supp Figure 1B). While this distinctive experimental paradigm is relatively low throughput, it has allowed us to investigate all these domains simultaneously.

It has previously been shown that electrophysiological responses upon whisking-based object detection saturate rapidly after a single whisker touch, whereas object localization may require multiple whisker touches[16,17], Correspondingly, when a single whisker is stimulated repeatedly, the response to the first pulse represents principally bottom-up thalamic-driven responses, whereas the later pulses in the train are expected to also gradually engage cortico-thalamo-cortical and cortico-cortical loops. We therefore first tested whether the initial pulses of the stimulus train (the first three out of total 20 pulses in 2s) evoked differential responses among the principal barrel, the adjacent septa, and the neighboring barrel upon SWS and MWS.

Earlier studies in which whisker-evoked responses were recorded either from barrel or from septa domains in separate experiments reported that the responses of barrel neurons to single principal whisker stimulation are much higher than those evoked in the

125 septal neurons[12,18]. The analysis of the data we obtained from the simultaneous
126 recordings at these domains, do not reveal such differences in first two pulse responses
127 among these columns in any of the laminae recorded upon single whisker stimulation
128 (SWS) (Figure 1D,G and J, First and Second Pulses). However response differences
129 emerged starting from the 3rd pulse upon SWS for L2/3 (Figure 1C,D and E, Third Pulse),
130 L4 (Figure 1F,G and H, Third Pulse) and L5 (Figure 1I,J and K, Third Pulse), and starting
131 from the 2nd pulse upon MWS in L4 (Supp. Figure 1E and F, Second Pulse), but not in
132 L2/3 or L5 (Supp. Figure 1C,D,G,H and I). While such differences also emerged between
133 stimulated principal and unstimulated neighboring barrels in L2/3 and L4 (starting at
134 different pulses; for L2/3: 7th pulse, for L4: 4th pulse, Figure1E and H, Barrel-vs-
135 Neighbour (BN) column), L5 did not show any significant difference (Figure 1K, BN
136 column). Interestingly, an inverted pattern of significant changes emerged between septa
137 and adjacent unstimulated neighboring barrels (Figure 1E, H and K, SN column). When
138 multiple whiskers were activated simultaneously, a divergence between barrel and septa
139 domains occured almost exclusively in Layer 4 (Supp. Figure 1I).
140
141 **SST+ and VIP+ neuron densities within Barrel and Septa Domains Diverge in Layer**
142 **4**
143
144 It is known that barrel and septa domains receive different thalamic projections, from VPM
145 and PoM respectively[19–22]. Our electrophysiological experiments show a significant
146 divergence of responses over time upon both SWS and MWS in L4 between barrels
147 (principal and neighboring) and adjacent septa that could be driven by this distinct
148 thalamocortical innervation or by differences in local circuitry. We therefore next assessed
149 the spatial distribution of local inhibitory cells in these domains, which could indicate their
150 active role in domain-specific activitation. Specifically, we made a comprehensive
151 analysis of the barrel versus septa localization of two inhibitory cell populations that
152 provide distinct regulation of cortical activity also in the temporal aspect, somatostatin
153 positive (SST+) and vasointestinal peptite positive (VIP+) cells.
154

Earlier research examining three inhibitory neuron populations in mouse barrel cortex showed that, while parvalbumin positive (PV+) cells do not show any differential density preference between barrel and septa columns, SST+ and VIP+ cells are significantly denser in the septa than in the barrels in L4[23]. Using a different strategy, we aimed to test the reported differential SST+ and VIP+ neuronal distributions. To label the two neuronal populations, we crossed the SST-Cre and VIP-Cre lines with a tdTomato reporter mouse line (Ai14). To comprehensively quantify the density of SST+ and VIP+ cells in the barrel and septa domains in 3D we utilized a passive CLARITY-based tissue clearing protocol, followed by light-sheet microscopy using a custom-built light-sheet microscope (mesoSPIM)[24,25]. The auto-fluorescence from the tissue was acquired with 488nm laser, which allows for the reliable detection of individual barrels in wS1, whereas the tdTomato positive SST+ or VIP+ neurons were detected by a 594nm laser, which permits us to localize and count cells in these two distinct domains accurately (Figure 2A and Supp. Figure 2). By adjusting the angle of each barrel column (in 3D using Imaris), we precisely identified the column of the barrel and septa in L2-3, L4 and L5, using the barrel borders for every plane (XY,YZ,XZ) in L4 (see Methods). Once the columns were accurately determined, we counted the number of tdTomato positive neurons in the barrels and septa and corresponding volumes for density estimation. We found that despite the known opposite distribution change along the depth of wS1 , both SST+ and VIP+ neuronal densities were higher in L4 septa compared to barrels, but we detected no difference in L2/3 and L5 (Figure 2B and C).

Based on the similarity of initial responses of all columns upon SWS and the subsequent divergence emerging over time (Figure 1C-K), as well as the confirmation that SST+ and VIP+ cell have higher densities in septa compared to barrel in L4 (Figure 2B and C), we wanted to identify potential temporal adaptation mechanisms present in SST+ or VIP+ interneurons that could cause such physiological differences.

Out of these two interneuron classes, SST+ interneurons tend to be more spontaneously active and supply powerful regulation to the local neuronal activity through dense feedback connections to nearby pyramidal neurons[26] In contrast, VIP+ interneurons

have been reported to exert their influence on network function via a dis-inhibitory circuit such that when driven by local, long-range, or neuromodulatory inputs, they inhibit SST+ interneurons (and to a lesser extent PV+ interneurons), resulting in reduced inhibition of pyramidal neurons[27–29].

SST+ and VIP+ interneurons exclusively express Elfn1 and the former contribute stronger to the temporal regulation

To explore potential genetic mechanisms that would be common to both SST+ and VIP+ inhibitory populations, which could contribute to the sensory adaptation observed, we performed gene expression analysis using the Allen Institute database[30] (Figure 3A). Subsequently, we also explored gene expression differences amongst all neuronal populations in three different databases to confirm identified candidates[31] (Figure 3B). To find gene with expression profiles that match closest to SST+ and VIP+ cells and furthest from excitatory cells (Exc) and parvalbumin positive (PV+) cell , we defined two distance metrics, combined correlation (CC) and combined p-value (Cp) (see Methods). This approach favors genes that are significantly correlated with the SST and VIP genes and uncorrelated with Exc and PV+ cell gene markers . In the Allen database, the Exc neuron marker included everything that expressed the Emx1 gene, whereas VIP, SST and PV genes were used for the respective neuronal populations. Although Emx1 is a developmental gene that may also label non-neuronal cell types, since we only considered neuronal expression, it does not pose a problem for our analysis.

We characterized five genes that have the highest CC and lowest Cp as potential contributors to the temporal adaptation profiles present in SST+ or VIP+ interneurons (Figure 3B and Supp. Figure 3A and B). Out of the five candidate genes that were common between the two SST+ and VIP+ populations of neurons, *Elfn1* is known to be involved in short-term plasticity and has been shown to affect the short-term excitatory input dynamics onto SST+ neurons[32].

Having identified *Elfn1* as the sole synaptic gene that is expressed in SST+ and VIP+ with known short-term plasticity effects, we went on to directly characterize the synaptic facilitation levels of excitatory inputs onto SST+ and VIP+ interneurons in WT and *Elfn1 knock-out (KO)* mice. We made acute slices from SST-Cre X tdTomato and VIP-Cre X tdTomato (Ai14) mice. Upon local neuropil stimulation and whole-cell recording from SST+ neurons in L2/3, we found a strong short-term facilitation of excitatory transmission in response to 10Hz neuropil stimulation (Figure 3C), which is in line with previous work[32,33]. When performing the same type of recordings from VIP+ cells, we found that genetic deletion of *Elfn1* also reduced the facilitation ratio at VIP interneurons (Multipolar, posthoc characterization). However, at 10 Hz, WT VIP+ multipolar cells displayed minimal facilitation, hence the loss of *Elfn1* produced synaptic depression instead (Figure 3D). Although 10 Hz represents the same frequency used for the whisker stimulation, closer examination of whisker evoked spiking, trace by trace, indicated that spiking consistency is low, thus comparisons between in vitro and in vivo data should be made cautiously. Nonetheless, the substantial reduction in facilitation for SST+ neurons, compared to multipolar VIP+ neurons, which comprise only a minority of the VIP+ population (the majority being bipolar, calretinin positive VIP+ neurons, which are unaffected in *Elfn1KO* mice[33]) suggest that any effect that the removal of *Elfn1* would have on the domain-dependent effects we observe in sensory-driven activity *in vivo,* would be dominated by its impact on SST+ neurons, and not on VIP+ ones.

Barrel-Septa response differences disappear in *Elfn1KO* mice

Having characterized physiological and anatomical differences between barrel and septa domains and having found a potential responsible gene for the physiological divergence between these anatomical domains, we next explored how the lack of *Elfn1* affects the sensory-driven activity *in vivo*.

Simultaneous recordings in barrel and septa domains in *Elfn1KO mice* upon SWS (Figure 4) and MWS (Supp. Figure 4) in fact revealed a lack of stimulus-dependent emerging differences between these domains found in WT controls upon SWS. While the

differences between barrels, septa and unstimulated neighbors upon SWS were largely diminished in L2/3 (Figure 4A,B and C) and L5 (Figure 4G,H and I), the observed differences in L4 between barrels and septa were not as strong between barrels and unstimulated neighbors (Figure 4D,E and F). Interestingly, response differences between barrel and septa domains upon MWS did not differ compared to WT controls, apart from the fact that the emergence of dissimilarities started at the 5th pulse as opposed to 2nd in WT (Supp. Figure 4G and 2I, respectively). This finding suggests that activity spillover from principal barrels is normally constrained by the delayed inhibition provided by the presence of *Elfn1* in excitatory synapses onto SST+ neurons, which have been shown to supply late recurrent inhibition in the cortex and hippocampus[32,34].

Barrels and Septa response identity is lost in *Elfn1KO* mice

It has been shown that the septal circuits are more sensitive to the frequency of whisker movements, which exemplifies the use of temporal vs rate coding of information in barrel and septa, respectively[14,15]. Hence it is conceivable that the existence of the septal regions separating the barrels provides a means to allow mice to separate these two interconnected yet very distinct information-processing routes along the temporal domain. In order to assess the information content of each of the two anatomical domains in WT animals and how it may change when activity between them converges in the *KO* animals, we trained a one-versus-all error-correcting output code (ECOC) classifier[35] with a GentleBoost[36] ensemble of decision trees using WT firing profile data from three domains (3-class classification). First, we performed 10-fold cross validation over the WT dataset (Figure 5A and B, left columns) and later we tested the WT-data-trained classifier with *Elfn1KO* firing profiles to compare the classifier performance.

The results show that in L2/3 and L4, barrel columns (Stimulated barrels and unstimulated neighbors) we get higher classification accuracy compared to septa for SWS data (Figure 5A, left column, L2/3 and L4), while L5 receiver operating characteristic (ROC) curves almost completely overlap for all conditions (Figure 5A, left columns, L5). Interestingly, while decoding accuracy for unstimulated neighbors was not drastically altered upon *KO*-

testing (Figure 5A, right column, all layers, turquoise), barrel and septa performances dropped significantly (Figure 5A, right column, gray and purple). This might not be surprising given that barrel, septa and neighbor response profiles are closer in Elfn1KO compared to WT (Supp. Figure 5A). We also saw that MWS-based decoders perform worse both for WT-crossvalidation and *KO* testing (Figure 5B) which is most likely due to the fact that barrel vs septa responses in WT animals are more similar to one another, while this is not the case for *Elfn1KO* animals (S5B Fig). However, most interestingly, layer 5 decoding performance completely drops to chance levels for the *KO*-test case (Figure 5B, L5, WT-Train, KO-Test).

It is quite interesting to observe that while response profiles of the tested domains got closer in *Elfn1KO* versus WT upon SWS (Supp. Figure 5A), the opposite happened upon MWS (Supp. Figure 5B).

wS1 Barrel Columns and Septal Domains have different wS2 and M1 Layer-dependent projection preferences

We identified that barrel and septa respond differently in WT mice and that this difference disappears in the *Elfn1KO* animals upon SWS and amplified upon MWS. Following up from this observation, we finally aimed to explore if the projection targets of these two wS1 domains are distinct, in a similar manner to what has been revealed for visual cortex domain projections[37]. By utilizing *in vivo* retrograde AAV injections in two of the main target cortical regions of wS1, we characterized the projections from wS1 to wS2 and M1.

We injected a retrograde AAV virus expressing GFP in wS2 or M1 in different mice (N=4 for S2 and N=6 for M1) and 4 weeks after the injection the brains were processed using passive tissue clearing and imaged using a custom-built light-sheet microscope (mesoSPIM) (Figure 6A). The auto-fluorescence of the barrels allowed for labeling of barrel columns in 3D, similar to our analysis on interneuron population distributions (Fig 2A and S2 Fig). We counted the number of neurons in wS1 barrel and septa domains

and measured the corresponding domain volumes to estimate projection densities as a proxy for connectivity levels between S1-S2 and S1-M1.

Our analysis showed that while barrels host significantly more wS2-projection cells in L2/3 (Figure 6B), septa domains host more M1-projecting neurons (Figure 6C). Overall our findings suggest that barrels verus septa domains do not only process distinct sensory-driven information regulated by local SST+ cell inhibition, but also transmit this information in a biased manner to downstream regions wS2 and M1.

Discussion

In the absence of visual stimuli, humans aim to identify an object by handling, with the first touch initiating the information accumulation process, and every subsequent touch leading to the full identification and characterization of the object, through evidence accumulation(Armstrong-James & Fox, 1987; Kheradpezhouh et al., 2017; Petersen, 2007).As is known, this process includes parrarel ascending pathways that bring the peripheral touch events through central pathways to the cortex in a somatotopic manner. Similarly, mice actively use their whiskers in place of arms and hands, again somatotopically mapping the whisker spatial pattern information one-to-one to the characterisitc cortical barrels.[40,41].

Although a large number of other species have whiskers, only a subset of animals with whiskers display a barrel pattern. For example, cats have whiskers and barrel-like structures in the brainstem nuclei (barrelettes) but have no barrels visible in their cortex[42–44]. It is the volitional whisking behavior that seems to correlate with an animal having barrels in their wS1 or not. The fact that animals whisk to identify surrounding structures and only have cortical barrels when they whisk, is suggestive of the importance of the one to one mapping in individual whisker information processing in the cortex. Here we find that septa play an important role in separating these parrarel whisker streams by regulating the lateral cortico-cortical information flow generated upon repetitive whisker touch. This process is tightly controlled by the short-term facilitation properties of

incoming input onto SST+ interneurons which is enabled by the expression of the Elfn1 gene.

It has previously been shown that, in contrast to L2/3 and L5/6, where SST+ cells are layer 1 targeting Martinotti type, the axons of SST+ INs in layer 4 of somatosensory cortex largely remain within layer 4[45]. In addition, while Martinotti cells receive facilitating synapses from PCs and form inhibitory synapses onto dendrites of neighboring PCs[46], non-Martinotti SST cells predominantly inhibit L4 FS cells in Layer 4[45,47]. Regarding the inputs onto the two L4 populations, SST+ and PV+ inhibitory cells are also activated in a divergent manner during thalamocortical activation at naturalistic whisking frequencies, with FS interneurons transiently excited due to the rapid depression of their thalamocortical inputs, whereas SST+ cells the opposite[48].

Somatosensation requires the accumulation of spatial and temporal information through repeated coordinated movement of corresponding sensory organs and these organs are often consisted of separate units such as hands and fingers or snout and whiskers. Although it has been speculated that the information relayed to and from barrels may differ from that of the septa[6,9,38], it has been unclear how this segregation is accomplished. The one-to-one topographic mapping of whiskers, thalamic barreloids, and cortical barrels favors an *a priori* assumption of bottom-up segregation of cortical domain identity. In contrast, our simultaneous recordings in the barrel and septa domains demonstrate that their sensory responses to the first whisker deflection do not significantly differ (Figure 1C-K). This would suggest that the first touch serves as an initiating signal in both domains, and it is only with repetitive activation of individual whiskers that their responses strongly diverge. Our work reveals that in addition to distinct feedforward thalamocortical projections, the cortical distribution of SST+ and VIP+ neurons (Figure 2) and the short-term synaptic dynamics onto SST+ interneurons (Figure 3) also contribute to this divergence and help shape cortical response identity. In our comparative gene analysis between septa-enriched and non-enriched cell types, we identified new gene candidates, including a long non-coding RNA of unknown function, for further study as potential mediators of differential response dynamics in wS1. Amongst the handful of

other genes found in our bioinformatics screen and based on previous work[32–34,49], *Elfn1* was a strong candidate for mediating a stimulius-dependent domain diversgence. Indeed we found that its removal abolishes the functional temporal divergence between barrel and septa domains (Figure 4). Thus, in addition to thalamo-cortical feedforward projections, we find that intracortical activity, shaped by SST+ inhibitory cells contributes to cortical domain response identity.

To further study if the spiking divergence in the temporal domain carries important sensory information, we trained an ECOC-based classifier to decode sensory stimuli among these separate yet interconnected domains. While the temporal profiles recorded at barrel domains upon SWS were successfully classified by the algorithm, the septal data was not (Figure 5A). These findings are consistent with previous suggestions that high dimensional temporal information (e.g., relating to object identity or location) is transmitted from wS1 to wS2 via the barrels, whereas low dimensional sensory information (e.g., object detection) is sent from wS1 to wM1 via septa[6,10,12,14,15]. Indeed, our retrograde labeling is consistent with this interpretation, with projection cells from wS1 barrels showing a bias to wS2, whereas projections from wS1 septa being biased to M1.When we instead examine multi-whisker stimulation, our sensory decoding from the classifier fails (Figure 5B), suggesting an impaired transmission of high dimensional data, at least in our experimental paradigm. Interestingly, the deletion of *Elfn1* decayed the ability of SWS to support sensory decoding which we attribute to the corresponding loss of SST+ interneuron contributions to frequency segregation. In addition, we saw a loss of differentiation between SW and MW stimuli and between barrel and septal regions (Figure 5A and Supp. Figure 5A and B).

Thus, in addition to any contributions from distinct thalamocortical input pathways, our findings reveal an important role for short-term plasticity driving cortical SST+ cell-mediated delayed inhibition in diversifying the response properties between individual barrels and septal regions, creating contrast in somatosensory information processing.

Acknowledgments

We thank members of the Karayannis lab for suggestions and comments on the manuscript. Authors also thank Rahel Kaestli for help with tissue clearing and light-sheet image acquisition.

Funding

This work was supported by Swiss National Science Foundation Grant S-41260-01-01 (T.K) and European Research Council Grant 679175 (T.K).

Author Contributions

Conceptualization: Ali Özgür Argunşah, Tevye Jason Stachniak, Jenq-Wei Yang, Theofanis Karayannis.
Data curation: Ali Özgür Argunşah, Tevye Jason Stachniak, Jenq-Wei Yang, Linbi Cai.
Formal analysis: Ali Özgür Argunşah, Tevye Jason Stachniak.
Funding acquisition: Theofanis Karayannis.
Investigation: Ali Özgür Argunşah, Tevye Jason Stachniak, Linbi Cai.
Methodology: Ali Özgür Argunşah, Tevye Jason Stachniak, Jenq-Wei Yang, Linbi Cai, George Kanatouris.
Project administration: Theofanis Karayannis.
Software: Ali Özgür Argunşah.
Supervision: Theofanis Karayannis.
Validation: Ali Özgür Argunşah, Tevye Jason Stachniak.
Visualization: Ali Özgür Argunşah, Tevye Jason Stachniak, Linbi Cai.
Mice: Tevye Jason Stachniak, Linbi Cai, George Kanatouris.
Immunohistochemistry: Tevye Jason Stachniak, Linbi Cai, George Kanatouris.
Writing – original draft: Ali Özgür Argunşah
Writing – review & editing: Ali Özgür Argunşah, Tevye Jason Stachniak, Theofanis Karayannis.

Declaration of Interest

The authors declare no competing interests.

Methods

RESOURCE AVAILABILITY

Lead Contact

Further information and requests for resources and reagents should be directed to and will be fulfilled by the Lead Contact, Theofanis Karayannis (karayannis@hifo.uzh.ch)

Materials Availability

This study did not generate new unique reagents.

Data and Code Availability

The datasets and analysis routines are available from the corresponding author on reasonable request.

Mice

All the animal experiments followed the guidelines of the Veterinary Office of Switzerland and were approved by the Cantonal Veterinary Office Zurich and the University of Zurich. husbandry with a 12-h reverse dark-light cycle (7 a.m. to 7 p.m. dark) at 24 °C and variable humidity. Adult (5- to 10-week-old) male C57BL6J wide type mice were used for retrograde tracing. Animal lines used in this study are VIP-IRES-Cre (Vip$^{tm1(cre)Zjh}$/J)[50], SST-IRES-Cre (Sst$^{tm2.1(cre)Zjh}$/J) [50], Ai14 (B6;129S6-Gt(ROSA)26Sor$^{tm14(CAG-tdTomato)Hze}$/J)[51] and HTB ((Gt(ROSA)26Sortm1(CAG-neo,-HTB)Fhg)[52], and Elfn1KO (Elfn1tm1(KOMP)Vlcg). Both male and female mice were used in cortical brain slice physiology and in vivo physiology experiments.

In-Vitro Electrophysiology

Whole-cell patch-clamp electrophysiological recordings were performed on labelled SST neurons located in neocortical layers 2/3 and 4 of barrel cortex (L2/3, L4, approximately bregma -0.5 to -2.0 mm) in acute brain slices prepared from postnatal day 7- 22 (P7–P22) male and female mice. Coronal brain slices from barrel cortex were prepared in cold

artificial cerebrospinal fluid (aCSF) containing (in mM): 128 NaCl, 26 NaHCO3, 10 D-glucose, 3 KCl, 1 MgCl2, 2 CaCl2 and 1.25 NaH2PO4, aerated with 95% O2 / 5% CO2. Acute slices were perfused at a rate of 2–3 ml/min with oxygenated ACSF at room temperature. Patch electrodes were made from borosilicate glass (Harvard Apparatus) and had a resistance of 2-4 MΩ. The intracellular solution had (in mM): 125 K gluconate, 2 KCl, 10 HEPES, 10 phosphocreatine, 4 MgCl2, 1 EGTA, 0.1 CaCl2, 4 ATP, 0.4 GTP, pH 7.35, 290 mOsm. Experiments were performed in voltage-clamp mode using the Axopatch 200B amplifier (Molecular Devices). Visually guided patch of fluorescent labelled cells was performed on a Zeiss Axioscope using a Retiga Electro camera (01-ELECTRO-M-14-C-OC, Teledyne Scientific Imaging). Access resistance was monitored to ensure the stability of recording conditions. Recordings with access resistance >40 MΩ, or whole cell capacitance <4 pF were excluded. No compensation was made for access resistance and no correction was made for the junction potential between the pipette and the ACSF. Following a baseline stabilization period (2-3 min), evoked synaptic currents recorded in 2 min (12 sweeps) at Vh= -70 mV were averaged and analyzed using Clampfit10 (Molecular Devices). Five electrical stimuli from a Digitimer isolated stimulator (DS2A Mk.II) were delivered at 50 Hz through a monopolar glass pipette (2-4 MΩ) positioned in L2/3, close to the soma of the recorded cells. The stimulating electrode was placed typically 100 - 250 µm from the recorded cell, parallel to the pial surface. A similar distance was maintained in L4 recordings, with the stimulating electrode parallel to the L2/3-L4 boundary. For the L2/3 to L4 recordings, the simulating electrode was then moved to lower L3 within the same column, again approximately 100 - 250 µm from the recorded cell but offset slightly to avoid directly stimulating the recorded cell's axon. Stimulation intensity and duration were adjusted to produce stable evoked EPSC amplitudes.

In-Vivo Silicon Probe Recording

We used 4 Elfn1KO and 4 WT littermates at the age of P20 to P30 for the multi-electrode recordings. Mice were anesthetized by urethane (1.5g/1kg) throughout the whole experiment. A heating pad was used to maintain the mouse's body temperature at 37°C. The depth of anesthesia was checked with breathing speed and paw reflexes throughout

the experiment. The skull of the right hemisphere was exposed by removing the skin on top, and a metallic head holder was implanted on the skull with cyanoacrylate glue and dental cement. A 20G needle was used to open a ~3mm x 3mm cranial window which exposed the S1 barrel field (wS1). Extreme care was taken not to cause damage or surface bleeding during surgery.

wS1 neural activities were recorded with an 8-shank-64-channel silicon probe. Each of the 8 shanks has 8 recording sites (100 µm apart). The distance between each shank is 200 µm (NeuroNexus Technologies, Ann Arbor, MI, USA). The silicon probe was labeled with DiI (1,1′-dioctadecyl-3,3,3′,3′-tetramethylindocarbocyanine, Molecular Probes, Eugene, OR, USA) and inserted perpendicularly into the barrel cortex. A silver wire was placed into the cerebellum as a ground electrode. All data were acquired at 20 kHz and stored with MC_RACK software (Multi Channel systems). The total duration of multi-electrode recordings varied between 3 h and 5 h. After each experiment, the animal was deeply anesthetized by ketamine (120 mg/kg, ketamine, 50 mg/mL, HamelnPharma, Hameln Germany) and perfused through the aorta with ringer solution. The brain was kept in 4% PFA. Tangential sections (200-µm thick) were prepared for cytochrome-oxidase (CO) histochemistry. By combining the DiI and CO staining, the insertion position of the 8 shank probes were identified in the barrel cortex. Only the shanks located within the identified individual barrels were used for the data analysis.

Whisker Stimulation

A single whisker was stimulated 1mm from the snout in rostral-to caudal direction (about 1mm displacement) using a stainless-steel rod (1 mm diameter) connected to a miniature solenoid actuator. The movement of the tip of the stimulator bar was measured precisely using a laser micrometer (MX series, Metralight, CA, USA) with a 2500 Hz sampling rate. The stimulus takes 26 ms to reach the maximal 1 mm whisker displacement, with a total duration of 60 ms until it reaches baseline (Yang et al., 2017). The whisker was stimulated at 10Hz for 2s. Each principal whisker in case of SWS and multiple whiskers at once in the case MWS was stimulated 20 times (20 trials).

Analysis of Silicon Probe Data

Extracellular silicon probe data were analyzed using a custom-made Matlab script (Matlab 2019a, Mathworks, MA, USA). The raw data signal was band-pass filtered (0.8-5 kHz) and the multi-unit activity (MUA) was extracted with the threshold of 7.5 times the standard deviation (SD) of baseline. The current source density (CSD) map was used to identify L2-3 and L4. The earliest CSD sink was identified as layer 4, followed by L2-3 (Reyes-Puerta et al., 2015; van der Bourg et al., 2017). MUA was smoothed using a Gaussian kernel (0 mean, 5ms sigma).

Decoder Analysis

We employed a classification approach utilizing error-correcting output codes (ECOC) models with a gentle adaptive boosting (GentleBoost) strategy to train classifiers. This method is particularly effective in handling imbalanced data and unequal misclassification costs.

Like Logit Boost, each weak learner in the ensemble fitted a regression model to response values, $y_n \in \{-1, +1\}$. The mean-squared error, stored in the FitInfo property of the ensemble object by fitcensemble, is computed as:

$$N \sum_{n=0}^{d} d(t)_n (y_n - h_t(x_n))^2$$

where, $d(t)_n$ represents observation weights at step t (summing up to 1), and $h_t(x_n)$ denotes predictions from the regression model h_t fitted to response values y_n. As the strength of individual learners diminishes, the weighted mean-squared error converges towards 1.

The training of classifiers utilized wild-type data. In the case of single whisker (SW) data, three classes were considered: barrel, septa, and neighbors. For multi-whisker (MW) data, two classes were defined: barrel and septa. Subsequently, Elfn1 knockout (KO) SW or MW data was introduced into the trained model to obtain predictions, respectively.

555

556 **Retrograde tracing and tissue processing**

557 Mice were anesthetized by isoflurane and a small craniotomy was made above the
558 injection site (M1 or S2). 200nl AAV24-retro GFP was injected in the M1 or S2. 4 weeks
559 after injection, the animals were transcardially perfused using 1X PBS and 4% PFA.
560 Following that, the whole brains were used for hydrogel-based tissue clearing by putting
561 in a hydrogel solution (1% PFA, 4% Acrylamide, 0.05% Bis) for 48h before the hydrogel
562 polymerization was induced at 37 C. Afterwards, the brains were put in 40ml of 8% SDS
563 and kept shaking at room temperature until the tissue was cleared sufficiently (around 2
564 months). Then the brains were washed 3 times in PBS and put into a self-made refractive
565 index matching solution (RIMS) for the last clearing step. They were left to equilibrate in
566 5ml of RIMS for at least 4 days at room temperature before being imaged.

567

568 **Imaging of injected brain**

569 After clearing, brains were imagined by a home-built mesoscale selective plane
570 illumination microscope (mesoSPIM). The detailed steps were described elsewhere
571 (Voigt, F.F et al, 2019). The images were acquired by laser 488nm & 561nm with 0.8X
572 magnification (pixel size: 8.23um) for the view of the whole brain and 2X magnification
573 (pixel size: 3.26um) for the view of the ipsilateral barrel cortex. 488nm laser was to acquire
574 the fluorescence of virus while 561nm was to acquire an auto-fluorescence background
575 to visualize barrels in the barrel cortex.

576

577 **Tissue Processing for Passive Clearing and Imaging**

578 The method used for hydrogel-based tissue clearing is explained in detail elsewhere [53].
579 Briefly, the animals were transcardially perfused using 1x PBS and Hydrogel solution (1%
580 PFA, 4% Acrylamide, 0.05% Bis). The collected brains were post-fixed for 48 h in a
581 Hydrogel solution (1% PFA, 4% Acrylamide, 0.05% Bis). Afterward, the Hydrogel
582 polymerization was induced at 37 °C. Following the polymerization, the brains were
583 immersed in 40 mL of 8% SDS and kept shaking at room temperature until the tissue was
584 cleared sufficiently (10–40 days depending on the animal's age). Finally, after 2–4 washes
585 in PBS, the brains were put into a self-made refractive index matching solution (RIMS)

[54]. They were left to equilibrate in 5 mL of RIMS for at least 4 days at RT (Room Temperature) before being imaged. After clearing, brains were attached to a small weight and loaded into a quartz cuvette, then submerged in RIMS, and imaged using a home-built mesoscale selective plane illumination microscope (mesoSPIM)[24]. The microscope consists of a dual-sided excitation path using a fiber-coupled multiline laser combiner (405, 488, 515, 561, 594, 647 nm, Omicron SOLE-6) and a detection path comprising an Olympus MVX-10 zoom macroscope with a 1× objective (Olympus MVPLAPO 1x), a filter wheel (Ludl 96A350), and a scientific CMOS (sCMOS) camera (Hamamatsu Orca Flash 4.0 V3). For imaging tdTomato and eGFP a 594 nm excitation with a 594 long-pass filter (594 LP Edge Basic, AHF) and 488 nm & 520/35 (BrightLine HC, AHF) were used respectively. The excitation paths also contain galvo scanners (GCM-2280-1500, Citizen Chiba) for light-sheet generation and reduction of streaking artifacts due to absorption of the light-sheet. In addition, the beam waist is scanning using electrically tunable lenses (ETL, Optotune EL-16-40-5D-TC-L) synchronized with the rolling shutter of the sCMOS camera. This axially scanned light-sheet mode (ASLM) leads to a uniform axial resolution across the field-of-view of 5–10 µm (depending on zoom and wavelength). The field of views ranged from 10.79 mm at ×1 or x0.8 magnification (Pixel size: 5.27 µm) for overview datasets. Further technical details of the mesoSPIM are described elsewhere[24,25]. The images generated with the mesoSPIM were preprocessed using Fiji and Imaris software to generate the images of the barrel cortex. For the quantification of neurons, the collected RAW files were converted to HDF5 format, and each z-plane was median filtered (window size 2 pixels) and convolved with a disc kernel (radius 1.5, convolution window size 10). The convolution was performed on the log-transformed z-plane and the convolution result was thresholded (threshold 0.3). On the convolved, thresholded z-planes local maxima were detected and then consolidated into cell detections in 3D space by matching and grouping detections on adjacent slices that are less than 5 pixels apart. Grouped detections were discarded if they spanned less than 4 adjacent slices. For the remaining grouped detections 3D cell positions were defined by the detection at median z location. 3D consolidated detections were filtered anatomically and morphologically using a semi-automated procedure to exclude non

cortical detections and detections not corresponding to neurons (e.g., blood vessels). Analysis was performed manually using Imaris

Analysis of cleared brain imaging data

Barrel cortex was imaged in 3D with 2X objective. The images were processed through Fiji and Imaris to visualize the 3D structure of the barrel cortex. XY-, YZ-, XZ- projections were visualized in Imaris, which allows us to adjust the correct angle for each barrel column to be vertical against XY-plane. This method allowed us identify barrel and septa in layers 2-3 and 5 and layer 4. In addition, the depth information is also precisely acquired for each barrel column. SST+ or VIP+ neuron numbers, S2-projected and M1-projected S1 neuron numbers were counted in icy. Max projection for each 50 ums along barrel columns was acquired and neurons on each max projection image were counted automatically by icy with the same threshold for all the brains. Each barrel was drawn according to the barrel map from each brain by max projection. The area of septa was calculated by subtracting the whole selected area from all the selected barrel areas.

Gene expression analysis

Two metrics were computed, Expression of all genes correlated with SST, VIP, PV and EMX genes and compared with ttest and plotted in 2D. Since we wanted high correlation and strong similarity with VIP and SST and the opposite for PV and Emx1, we used a combined similarity and correlation scores using the following formulas, Cp = pSST*pVIP*(1-pPV)*(1-pEMX), where pSST is the p value came out of a ttest between all genes and SST etc. CC = cSST*cVIP*(1-cPV)*(1-cEMX) where cSST is the correlation between SST gene and all genes.

Statistical Analysis

Data are represented as mean ± SEM unless stated otherwise. Statistical comparisons have been done using a one-tailed Mann-Whitney-U test. In the case of the Gaussian cluster analysis, a two-tailed t-test was applied on the epsilon distance between starter cells and pre-synaptic partners to check the statistical significance threshold was set to $p<0.05$; in the Figures, different degrees of evidence against the null hypothesis are

indicated by asterisks (p<0.05: *; p<0.01: **; p<0.001: ***). Cell densities in Figure 2 and 6 were compared using repeated measures ANOVA. All tests were conducted using custom codes in Matlab.

Figures Legends

Figure 1. Layer specific temporal divergences emerge in barrel and septa domains upon repeated single-whisker stimulation. (A) Acute *in-vivo* silicon probe (8x8) recordings were performed after the start of active whisking (>P21). Principal whiskers were stimulated one by one for 2s at 10Hz. (B) Left: Probe locations were labeled after each experiment using histology. Right: Only the triplets of electrodes were used in the analysis in which principal barrel (B), adjacent septa (S) and the adjacent neighboring barrel (N) were captured by the probe insertion sites for any experiment. 14 barrel columns, 9 septal columns, 18 unstimulated neighboring barrels from N=4 mice. (C) Analysis for Layer 2/3. Left: Average firing profiles of barrel (black), unstimulated neighbor (blue) and septa (pink) columns upon 2s-long 10Hz repeated whisker stimulation. Middle: Average firing rates per stimulating pulse. Right: Average firing rates for 1st, 2nd, 3rd, and 20th pulses zoomed in. (D) Pair-wise statistical comparisons of three conditions for 1st, 2nd, 3rd, and 20th pulses (Mann-Whitney-U-Test). (E) Pair-wise statistical comparisons of three conditions for all pulses (Mann-Whitney-U-Test). (F-G-H) Same with C-D-E but for Layer 4. (I-J-K) Same with C-D-E but for Layer 5. (*: p<0.05; **: p<0.01;***:p<0.001; Dark shading is a function of p value and white stands for p>0.05.)

Figure 2. SST+ and VIP+ neuron densities differ at Barrel and Septa Domains in Layer 4. (A) A passive CLARITY-based tissue clearing protocol was performed on the collected brains which were subsequently imaged in their entirety using a custom-built light-sheet microscope (mesoSPIM). 594nm wavelength was used to image tdTomato, 488nm wavelength was used to image autofluorescence. (B) SST+ neuron density distribution over laminae for barrel and septal domains (N=4 mice, n=54 Barrels and surrounding septa per barrel). Normalized cell densities plotted as a function of depth. 0µm represents the top of layer 4. SST+ interneuron density is significantly higher in septa

(p=0.0015, F=30.64, repeated-measures ANOVA). (C) VIP+ neuron density distribution over laminae for barrel and septal domains. (N=4 mice, n= 53 Barrels and surrounding septa per barrel). Normalized cell densities plotted as a function of depth. 0µm represents the top of layer 4. VIP+ interneuron density is also significantly higher in septa (p=0.0.21, F=9.63, repeated-measures ANOVA)

Figure 3. Elfn1 is predominantly expressed in SST+ and VIP+ Interneurons and responsible for the short-term plasticity related temporal engagement. (A) Scatter plot showing genes exclusively expressed by SST+ and VIP+ neurons only. X-axis is the combined correlation which is calculated as follows: cSST.*cVIP.*(1-cPV).*(1-cEXC), where cX represents the correlation between the test sequence and the neuronal type of interest X. This formula favors genes that are highly expressed in SST and VIP cells and not expressed in Exc and PV cells. The higher the combined correlation, the better. Similarly, Y-Axis is the combined p-value which is calculated as follows pSST.*pVIP.*(1-pPV).*(1-pEXC), where pX represents the p-value (two-sample t-test) between the test sequence and the neuronal type of interest X. This formula favors genes that significantly similar with SST and VIP cells and different from Exc and PV cells. Lower the combined p-value, better. (B) Elfn1 gene expression data across three RNA-seq datasets containing cortical excitatory neurons and inhibitory interneuron subtypes visualized as boxplots of RPKM expression levels. Boxes show median and interquartile ranges, and whiskers show full data without outliers. (C) Excitatory synaptic events evoked by repetitive local electrical stimulation produce strongly facilitating EPSCs onto SST interneurons. At 10 Hz, this is principally due to a suppression of initial release probability. For wildtype SST interneurons EPSCs facilitate rapidly at 10 Hz ($p=0.003$, 3×10^{-7}, 3×10^{-11} and 3×10^{-15} for 2^{nd} 3^{rd} 4^{th} and 5^{th} stimuli vs 1^{st} stimuli, respectively). Elfn1 knockout removes this facilitation (P = 1, 1, 1, 1 vs 1^{st}). Responses in KO neurons facilitate less than in WT neurons ($P= 0.0001$, 6×10^{-7} for 4^{th} and 5^{th} stimuli ANOVA with Bonferroni post hoc). (D) Elfn1 KO also alters ESPC facilitation ratio onto multipolar VIP interneurons at 10 Hz. Wildtype VIP interneurons do not display substantial facilitation at 10 Hz (p=1, 1, 1 and 1 for 2^{nd} 3^{rd} 4^{th} and 5^{th} stimuli vs 1^{st} stimuli, respectively). Elfn1 knockout induces synaptic depression ($p=1{,}6 \times 10^{-4}$, 5×10^{-6}, 1×10^{-6} vs 1^{st}). Responses in KO neurons depress more

than in WT neurons (p=0.03, 0.0004, 0.001 for 3rd, 4th, and 5th stimuli ANOVA with Bonferroni post hoc). *p<0.05, **p<0.01, ***p<0.001

Figure 4. Loss of Elfn1 abolishes barrel-septa response divergences upon single-whisker stimulation. (A) Analysis for Layer 2/3. Left: Average firing profiles of barrel (gray), unstimulated neighbor (turquois) and septa (purple) columns upon 2s-long 10Hz repeated whisker stimulation. Middle: Average firing rates per stimulating pulse (11 barrel columns, 7 septal columns, 11 unstimulated neighbors from N=4 mice.). Right: Average firing rates for 1st, 2nd, 3rd, and 20th pulses. (B) Pair-wise statistical comparisons of three conditions for four pulses. (C) Pair-wise statistical comparisons of three conditions for all pulses. (D-E-F) Same with A-B-C but for Layer 4. (G-H-I) Same with A-B-C but for Layer 5. (*: p<0.05; **: p<0.01;***:p<0.001; Two-sided Mann-Whitney U Test. White represents p>0.05.)

Figure 5. Decoding analysis shows an alteration of columnar domain identity in *Elfn1KO* animals. (A) Decoder analysis based on the single whisker stimulation response profiles. Left column represents the receiver operating characteristic (ROC) curve of the classification performance of the decoder trained and cross-validated using WT data. Right column represents the ROC curve of the classification performance after training with WT and testing with KO data. (B) Decoder analysis based on the multi whisker stimulation response profiles. Left column represents the receiver operating characteristic (ROC) curve of the classification performance of the decoder trained and cross-validated using multi-whisker WT data. Right column represents the ROC curve of the classification performance after training with WT and testing with KO data.

Figure 6. wS1 barrel and septa columns differentially project to wS2 and M1 (A) The representation of the experimental protocol and timelines. The retro-AAV-CAG-GFP was injected in either S2, or M1 at P20-30 and the brains were dissected 4 weeks after the virus injection following the tissue clearing and whole brain imaging. (B) Normalized cell density profiles of S2 and M1 projection neurons at barrel columns. 0µm represents the top of layer 4. Layer 2/3-barrel columns send significantly more projections to S2

(p=0.0293, F=7.02, repeated-measures ANOVA). (C) Normalized cell density profiles of S2 and M1 projections neurons at septa columns. 0µm represents the top of layer 4. Layer 5 septal columns send significantly more projections to M1 (p=0.0402, F=5.98, repeated measures ANOVA).

Supplementary Figure Legends

Supplementary Figure 1. Layer 4 presents the highest level of temporal divergences between barrel and septa domains upon repeated multi-whisker stimulation. (A) Acute *in-vivo* silicon probe (8x8) recordings were performed after the start of active whisking (>P21). Most of the principal whiskers were stimulated for 2s at 10Hz. (B) Left: Probe locations were labeled after each experiment using histology. Right: Only the triplets of electrodes were used in the analysis in which principal barrel (B), adjacent septa (S) and the adjacent neighboring barrel (N) were captured by the probe insertion sites for single whisker stimulation experiments. Only barrels and septa were used for multi whisker analysis. 14 barrel columns, 9 septal columns from n=4 mice. (C) Analysis for Layer 2/3. Left: Average firing profiles of barrel (black) and septa (pink) columns upon 2s-long 10Hz repeated whisker stimulation. Middle: Average firing rates per stimulating pulse. Right: Average firing rates for 1st, 2nd, 3rd, and 20th pulses. (D) Pair-wise statistical comparisons of three conditions for four pulses. (E-F) Same with C-D but for Layer 4. (G-H) Same with C-D but for Layer 5. (I) Barrel-Septa comparison for Layer 2/3,4 and 5 (*: p<0.05; **: p<0.01;***:p<0.001; Two-sided Mann-Whitney U Test. White represents p>0.05.)

Supplementary Figure 2. SST+ and VIP+ neuron densities differ at Barrel and Septa Domains in Layer 4. Left: Example SST-tdTomato brain virtual slice on left. Right Top: Inner ring represents barrel borders; outer ring represents septal borders. Right Bottom: Same as top but without green channel.

Supplementary Figure 3. Elfn1 is solely expressed in SST+ and VIP+ Interneurons and responsible for the short-term plasticity related temporal engagement. (A) Each

bar shows the differential expression of Elfn1 in a comparison within one of the datasets. Fold-Changes are relative to the other 3 groups of neuron subtypes within the same dataset. (B) Gene expression data for other four candidates across three RNA-seq datasets containing cortical excitatory neurons and inhibitory interneuron subtypes. Each dot represents a single sample.

Supplementary Figure 4. Loss of Elfn1 does not alter barrel-septa response profiles upon multi-whisker stimulation. (A) Analysis for Layer 2/3. Left: Average firing profiles of barrel (gray) and septa (purple) columns upon 2s-long 10Hz repeated whisker stimulation. Middle: Average firing rates per stimulating pulse (11 barrel columns, 7 septal columns from n=4 mice.)). Right: Average firing rates for 1st, 2nd, 3rd, and 20th pulses. (B) Pair-wise statistical comparisons of three conditions for four pulses. (C-D) Same with A-B but for Layer 4. (E-F) Same with A-B but for Layer 5. (G) Barrel-Septa comparison for Layer 2/3,4 and 5 (*: $p<0.05$; **: $p<0.01$;***:$p<0.001$; Two-sided Mann-Whitney U Test. White represents $p>0.05$.)

Supplementary Figure 5. Visual presentation of WT vs Elfn1KO response profiles. (A) Visual comparison of mean firing rates of WT vs KO SWS responses for all three conditions and layers. (B) Visual comparison of mean firing rates of WT vs KO MWS responses for both conditions and all layers.

References

1. Douglas RJ, Martin KAC. Neuronal circuits of the neocortex. Annual Review of Neuroscience. 2004. doi:10.1146/annurev.neuro.27.070203.144152
2. Horton JG, Adams DL. The cortical column: A structure without a function. Philosophical Transactions of the Royal Society B: Biological Sciences. 2005. doi:10.1098/rstb.2005.1623
3. Harris KD, Mrsic-Flogel TD. Cortical connectivity and sensory coding. Nature. 2013. doi:10.1038/nature12654
4. Kim U, Ebner FF. Barrels and septa: Separate circuits in rat barrel field cortex. Journal of Comparative Neurology. 1999;408. doi:10.1002/(SICI)1096-9861(19990614)408:4<489::AID-CNE4>3.0.CO;2-E

5. Bureau I, Von Paul F Saint, Svoboda K. Interdigitated paralemniscal and lemniscal pathways in the mouse barrel cortex. PLoS Biol. 2006;4. doi:10.1371/journal.pbio.0040382
6. Alloway KD. Information processing streams in rodent barrel cortex: The differential functions of barrel and septal circuits. Cerebral Cortex. 2008. doi:10.1093/cercor/bhm138
7. Staiger JF, Petersen CCH. Neuronal circuits in barrel cortex for whisker sensory perception. Physiol Rev. 2021;101. doi:10.1152/physrev.00019.2019
8. Shepherd GMG, Svoboda K. Laminar and columnar organization of ascending excitatory projections to layer 2/3 pyramidal neurons in rat barrel cortex. Journal of Neuroscience. 2005;25. doi:10.1523/JNEUROSCI.1173-05.2005
9. Chakrabarti S, Alloway KD. Differential origin of projections from SI barrel cortex to the whisker representations in SII and MI. Journal of Comparative Neurology. 2006;498. doi:10.1002/cne.21052
10. Sato TR, Svoboda K. The functional properties of barrel cortex neurons projecting to the primary motor cortex. Journal of Neuroscience. 2010;30. doi:10.1523/JNEUROSCI.3774-09.2010
11. Audette NJ, Urban-Ciecko J, Matsushita M, Barth AL. POm Thalamocortical Input Drives Layer-Specific Microcircuits in Somatosensory Cortex. Cereb Cortex. 2018;28. doi:10.1093/cercor/bhx044
12. Brecht M, Sakmann B. Dynamic representation of whisker deflection by synaptic potentials in spiny stellate and pyramidal cells in the barrels and septa of layer 4 rat somatosensory cortex. Journal of Physiology. 2002. doi:10.1113/jphysiol.2002.018465
13. Cai L, Yang JW, Wang CF, Chou SJ, Luhmann HJ, Karayannis T. Identification of a Developmental Switch in Information Transfer between Whisker S1 and S2 Cortex in Mice. Journal of Neuroscience. 2022;42. doi:10.1523/JNEUROSCI.2246-21.2022
14. Melzer P, Champney GC, Maguire MJ, Ebner FF. Rate code and temporal code for frequency of whisker stimulation in rat primary and secondary somatic sensory cortex. Exp Brain Res. 2006;172: 370–386. doi:10.1007/s00221-005-0334-1
15. Melzer P, Sachdev RNS, Jenkinson N, Ebner FF. Stimulus frequency processing in awake rat barrel cortex. Journal of Neuroscience. 2006;26. doi:10.1523/JNEUROSCI.2620-06.2006
16. O'Connor DH, Hires SA, Guo Z V., Li N, Yu J, Sun QQ, et al. Neural coding during active somatosensation revealed using illusory touch. Nat Neurosci. 2013;16. doi:10.1038/nn.3419
17. Pammer L, O'Connor DH, Hires SA, Clack NG, Huber D, Myers EW, et al. The mechanical variables underlying object localization along the axis of the whisker. Journal of Neuroscience. 2013;33. doi:10.1523/JNEUROSCI.4316-12.2013
18. Armstrong-James M, Fox K. Spatiotemporal convergence and divergence in the rat S1 "Barrel" cortex. Journal of Comparative Neurology. 1987;263. doi:10.1002/cne.902630209
19. Koralek KA, Jensen KF, Killackey HP. Evidence for two complementary patterns of thalamic input to the rat somatosensory cortex. Brain Res. 1988;463. doi:10.1016/0006-8993(88)90408-8
20. Chmielowska J, Carvell GE, Simons DJ. Spatial organization of thalamocortical and corticothalamic projection systems in the rat SmI barrel cortex. Journal of Comparative Neurology. 1989;285. doi:10.1002/cne.902850304

21. Ahissar E, Sosnik R, Bagdasarian K, Haidarliu S. Temporal frequency of whisker movement. II. Laminar organization of cortical representations. J Neurophysiol. 2001;86. doi:10.1152/jn.2001.86.1.354
22. Sosnik R, Haidarliu S, Ahissar E. Temporal frequency of whisker movement. I. Representations in brain stem and thalamus. J Neurophysiol. 2001;86. doi:10.1152/jn.2001.86.1.339
23. Almási Z, Dávid C, Witte M, Staiger JF. Distribution patterns of three molecularly defined classes of gabaergic neurons across columnar compartments in mouse barrel cortex. Front Neuroanat. 2019;13. doi:10.3389/fnana.2019.00045
24. Voigt FF, Kirschenbaum D, Platonova E, Pagès S, Campbell RAA, Kastli R, et al. The mesoSPIM initiative: open-source light-sheet microscopes for imaging cleared tissue. Nat Methods. 2019;16. doi:10.1038/s41592-019-0554-0
25. Vladimirov N, Voigt F, Naert T, Araujo GR, Cai R, Reuss AM, et al. The Benchtop mesoSPIM: a next-generation open-source light-sheet microscope for large cleared samples. bioRxiv. 2023.
26. Urban-Ciecko J, Barth AL. Somatostatin-expressing neurons in cortical networks. Nat Rev Neurosci. 2016;17. doi:10.1038/nrn.2016.53
27. Lee S, Kruglikov I, Huang ZJ, Fishell G, Rudy B. A disinhibitory circuit mediates motor integration in the somatosensory cortex. Nat Neurosci. 2013;16. doi:10.1038/nn.3544
28. Pi HJ, Hangya B, Kvitsiani D, Sanders JI, Huang ZJ, Kepecs A. Cortical interneurons that specialize in disinhibitory control. Nature. 2013;503. doi:10.1038/nature12676
29. Karnani MMM, Jackson J, Ayzenshtat I, Tucciarone J, Manoocheri K, Snider WGG, et al. Cooperative Subnetworks of Molecularly Similar Interneurons in Mouse Neocortex. Neuron. 2016;90. doi:10.1016/j.neuron.2016.02.037
30. Yao Z, van Velthoven CTJ, Nguyen TN, Goldy J, Sedeno-Cortes AE, Baftizadeh F, et al. A taxonomy of transcriptomic cell types across the isocortex and hippocampal formation. Cell. 2021;184. doi:10.1016/j.cell.2021.04.021
31. Huntley MA, Srinivasan K, Friedman BA, Wang TM, Yee AX, Wang Y, et al. Genome-wide analysis of differential gene expression and splicing in excitatory neurons and interneuron subtypes. Journal of Neuroscience. 2020;40. doi:10.1523/JNEUROSCI.1615-19.2019
32. Stachniak TJ, Sylwestrak EL, Scheiffele P, Hall BJ, Ghosh A. Elfn1-induced constitutive activation of mglur7 determines frequency-dependent recruitment of somatostatin interneurons. Journal of Neuroscience. 2019;39. doi:10.1523/JNEUROSCI.2276-18.2019
33. Stachniak TJ, Kastli R, Hanley O, Argunsah AÖ, Van Der Valk EGT, Kanatouris G, et al. Postmitotic prox1 expression controls the final specification of cortical VIP interneuron subtypes. Journal of Neuroscience. 2021;41. doi:10.1523/JNEUROSCI.1021-21.2021
34. Tomioka NH, Yasuda H, Miyamoto H, Hatayama M, Morimura N, Matsumoto Y, et al. Elfn1 recruits presynaptic mGluR7 in trans and its loss results in seizures. Nat Commun. 2014;5. doi:10.1038/ncomms5501
35. Allwein EL, Schapire RE, Singer Y. Reducing multiclass to binary: A unifying approach for margin classifiers. Journal of Machine Learning Research. 2001;1.
36. Friedman J, Hastie T, Tibshirani R. Additive logistic regression: A statistical view of boosting. Annals of Statistics. 2000. doi:10.1214/aos/1016218223

37. Meier AM, Wang Q, Ji W, Ganachaud J, Burkhalter A. Modular network between postrhinal visual cortex, amygdala, and entorhinal cortex. Journal of Neuroscience. 2021;41. doi:10.1523/JNEUROSCI.2185-20.2021
38. Petersen CCH. The functional organization of the barrel cortex. Neuron. 2007. doi:10.1016/j.neuron.2007.09.017
39. Kheradpezhouh E, Adibi M, Arabzadeh E. Response dynamics of rat barrel cortex neurons to repeated sensory stimulation. Sci Rep. 2017;7. doi:10.1038/s41598-017-11477-6
40. Van Der Loos H, Woolsey TA. Somatosensory cortex: Structural alterations following early injury to sense organs. Science (1979). 1973;179. doi:10.1126/science.179.4071.395
41. Woolsey TA, Welker C, Schwartz RH. Comparative anatomical studies of the Sml face cortex with special reference to the occurrence of “barrels” in layer IV. Journal of Comparative Neurology. 1975;164. doi:10.1002/cne.901640107
42. Rice FL, Gomez C, Barstow C, Burnet A, Sands P. AComparative analysis of the development of the primary somatosensory cortex: Interspecies similarities during barrel and laminar development. Journal of Comparative Neurology. 1985;236. doi:10.1002/cne.902360405
43. Rice FL. An attempt to find vibrissa-related barrels in the primary somatosensory cortex of the cat. Neurosci Lett. 1985;53. doi:10.1016/0304-3940(85)90180-6
44. Nomura S, Itoh K, Sugimoto T, Yasui Y, Kamiya H, Mizuno N. Mystacial vibrissae representation within the trigeminal sensory nuclei of the cat. Journal of Comparative Neurology. 1986;253. doi:10.1002/cne.902530110
45. Xu H, Jeong HY, Tremblay R, Rudy B. Neocortical Somatostatin-Expressing GABAergic Interneurons Disinhibit the Thalamorecipient Layer 4. Neuron. 2013;77. doi:10.1016/j.neuron.2012.11.004
46. Silberberg G, Markram H. Disynaptic Inhibition between Neocortical Pyramidal Cells Mediated by Martinotti Cells. Neuron. 2007;53. doi:10.1016/j.neuron.2007.02.012
47. Ma Y, Hu H, Berrebi AS, Mathers PH, Agmon A. Distinct subtypes of somatostatin-containing neocortical interneurons revealed in transgenic mice. Journal of Neuroscience. 2006;26. doi:10.1523/JNEUROSCI.0661-06.2006
48. Tan Z, Hu H, Huang ZJ, Agmon A. Robust but delayed thalamocortical activation of dendritic-targeting inhibitory interneurons. Proc Natl Acad Sci U S A. 2008;105. doi:10.1073/pnas.0710628105
49. Stachniak TJ, Argunsah AÖ, Yang J-W, Cai L, Karayannis T. Presynaptic kainate receptors onto somatostatin interneurons are recruited by activity throughout development and contribute to cortical sensory adaptation. Journal of Neuroscience. 2023;43. doi:10.1523/JNEUROSCI.1461-22.2023
50. Taniguchi H, He M, Wu P, Kim S, Paik R, Sugino K, et al. A Resource of Cre Driver Lines for Genetic Targeting of GABAergic Neurons in Cerebral Cortex. Neuron. 2011;71: 995–1013. doi:10.1016/j.neuron.2011.07.026
51. Madisen L, Zwingman TA, Sunkin SM, Oh SW, Zariwala HA, Gu H, et al. A robust and high-throughput Cre reporting and characterization system for the whole mouse brain. Nat Neurosci. 2010;13: 133–140. doi:10.1038/nn.2467
52. Li Y, Stam FJ, Aimone JB, Goulding M, Callaway EM, Gage FH. Molecular layer perforant path-associated cells contribute to feed-forward inhibition in the adult dentate

gyrus. - Supporting Information. Proc Natl Acad Sci U S A. 2013;110: 9106–11. doi:10.1073/pnas.1306912110

53. Chung K, Deisseroth K. CLARITY for mapping the nervous system. Nat Methods. 2013;10. doi:10.1038/nmeth.2481

54. Yang B, Treweek JB, Kulkarni RP, Deverman BE, Chen CK, Lubeck E, et al. Single-cell phenotyping within transparent intact tissue through whole-body clearing. Cell. 2014;158. doi:10.1016/j.cell.2014.07.017

Figures

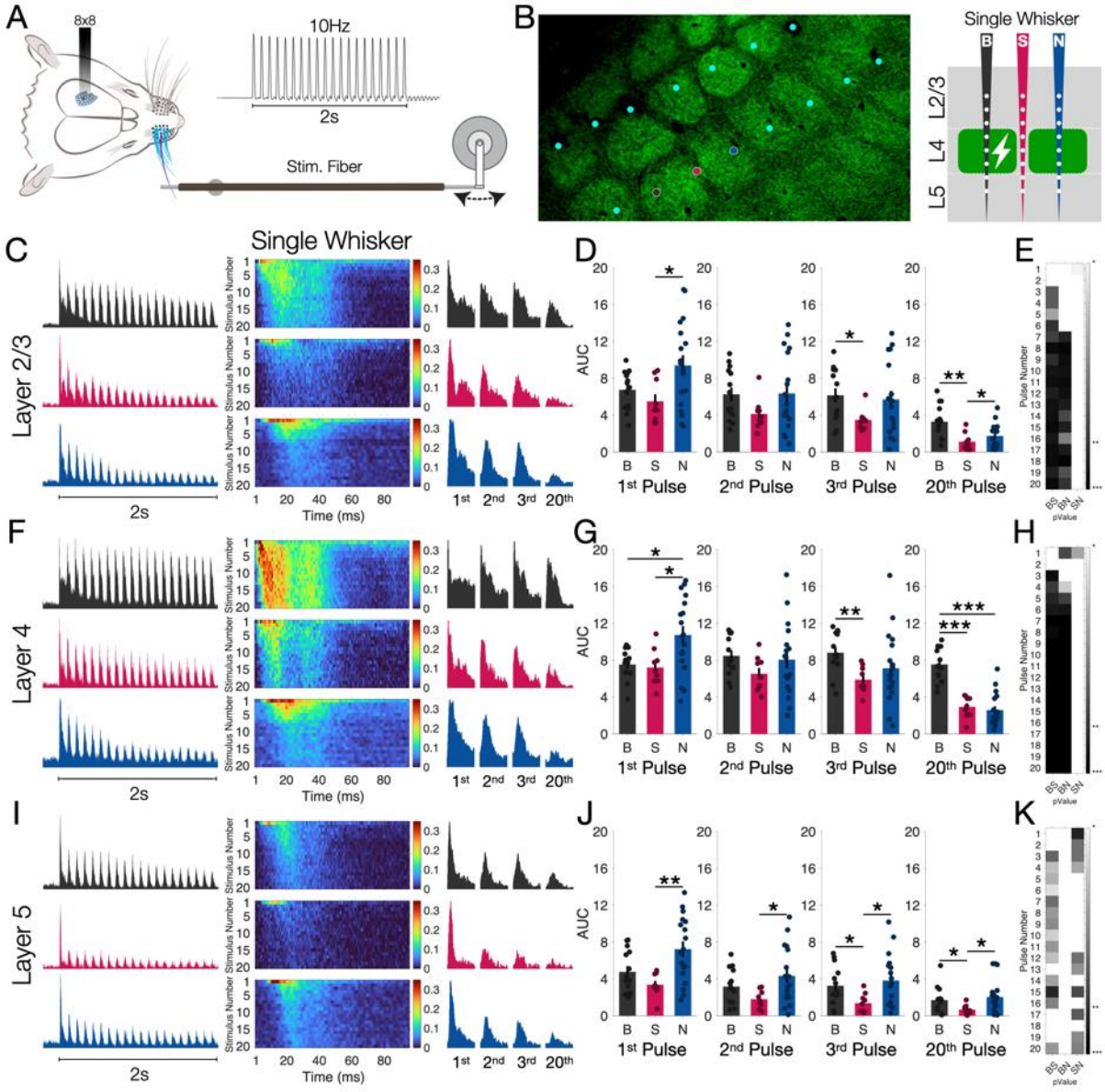

Figure 1, Argunsah et al., 2024

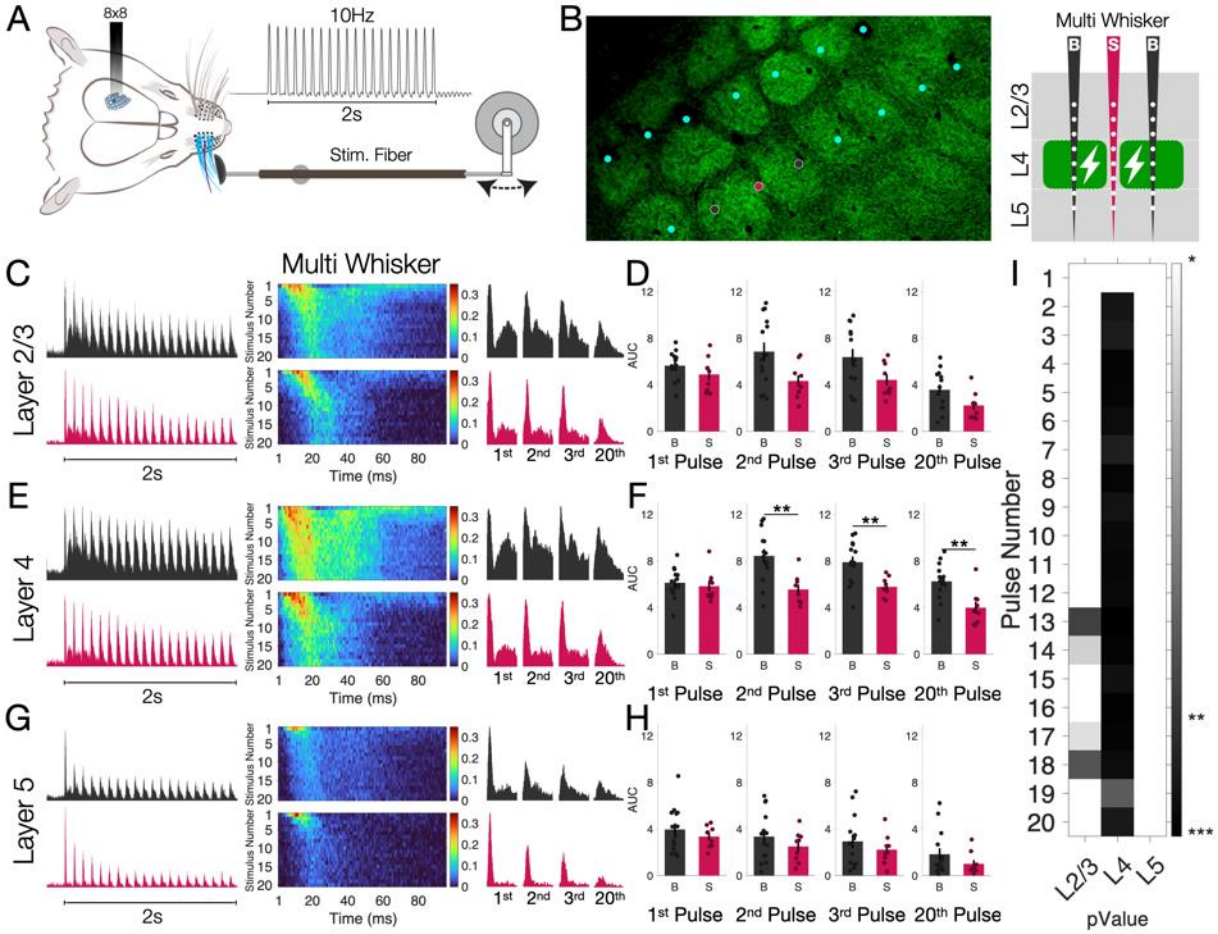

Supplementary Figure 1, Argunsah et al., 2024

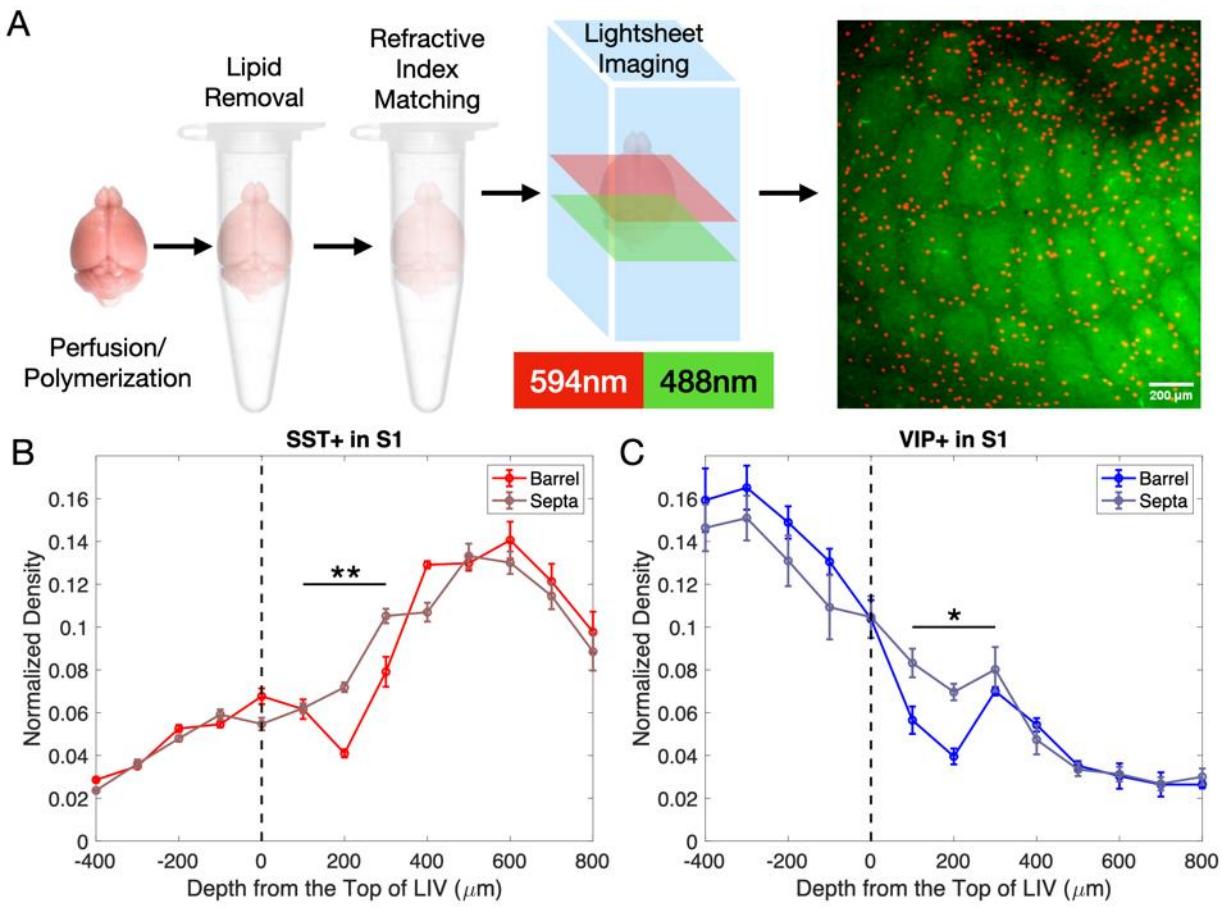

Figure 2, Argunsah et al., 2024

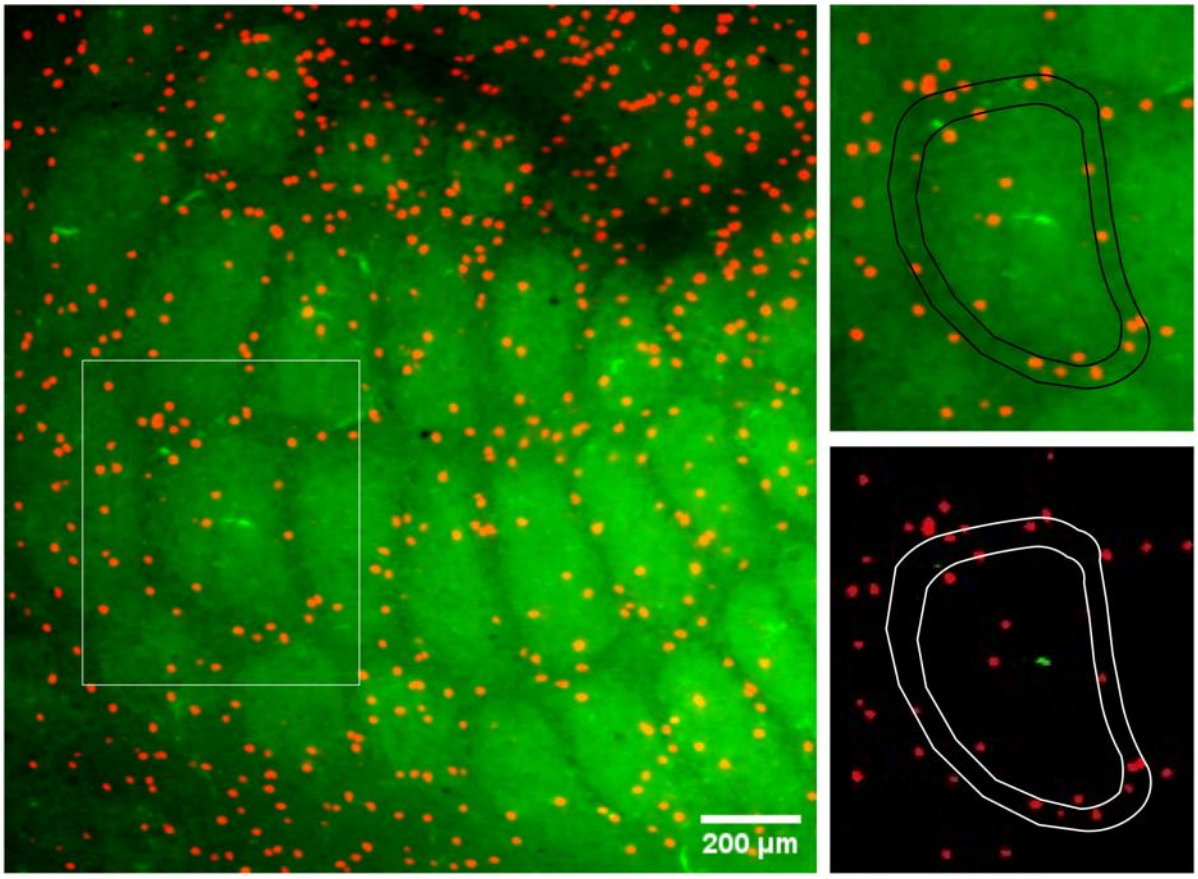

Supplementary Figure 2, Argunsah et al., 2024

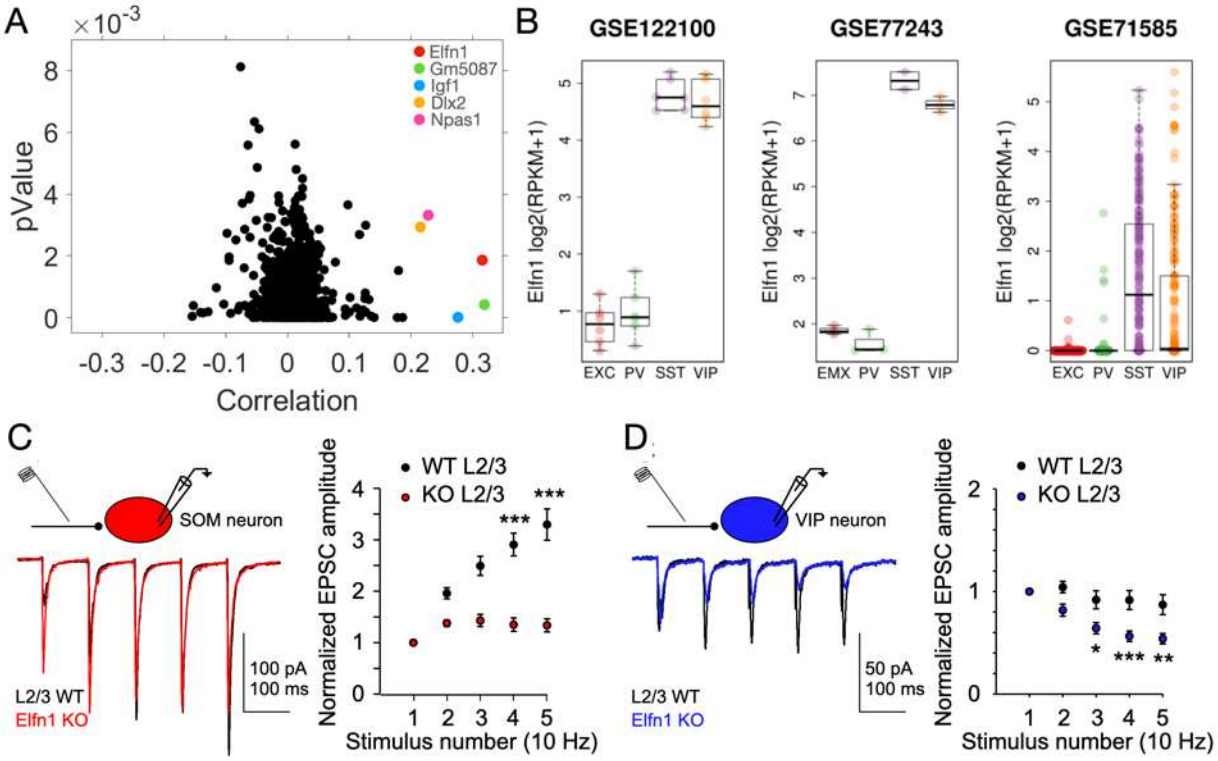

Figure 3, Argunsah et al., 2024

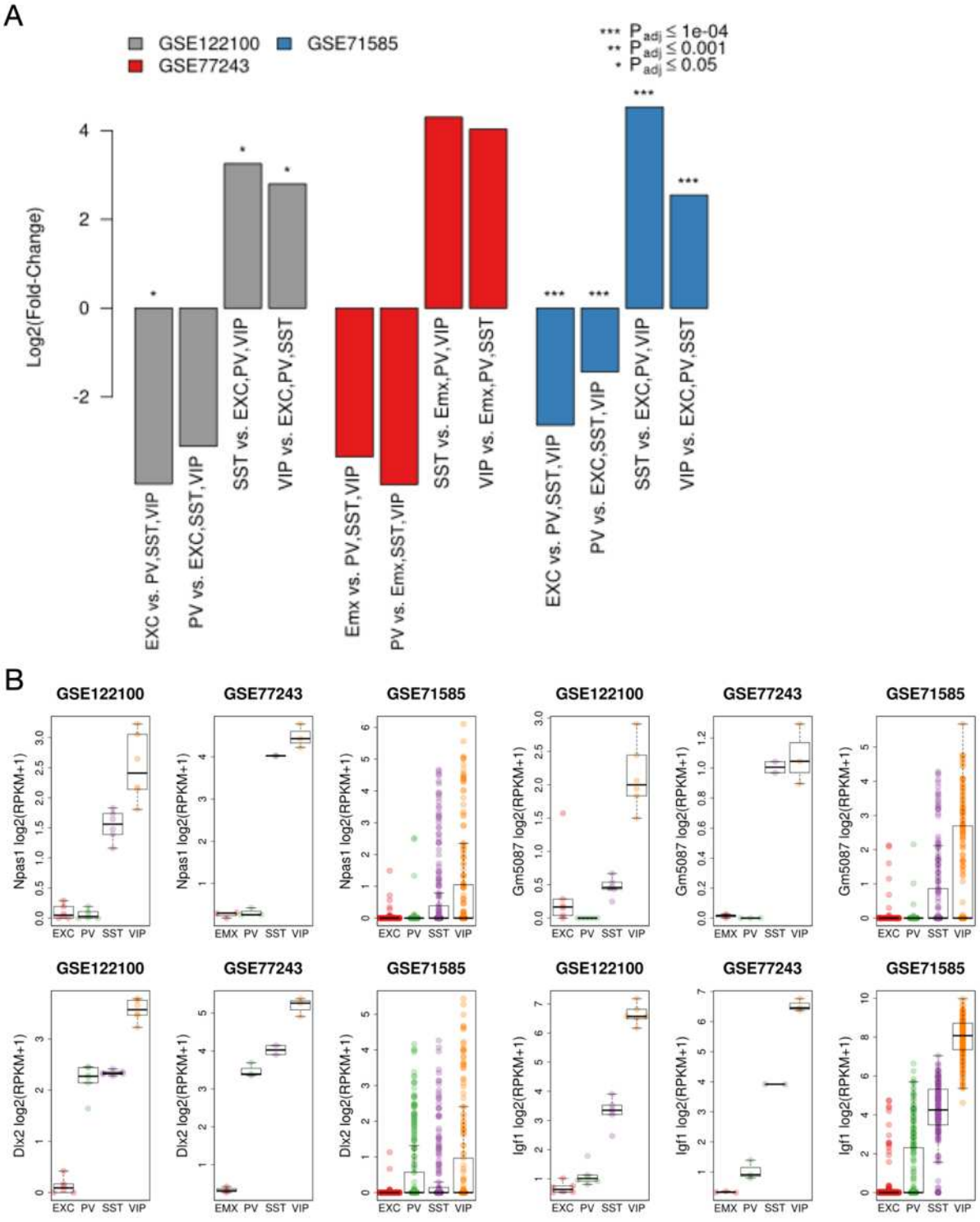

Supplementary Figure 3, Argunsah et al., 2024

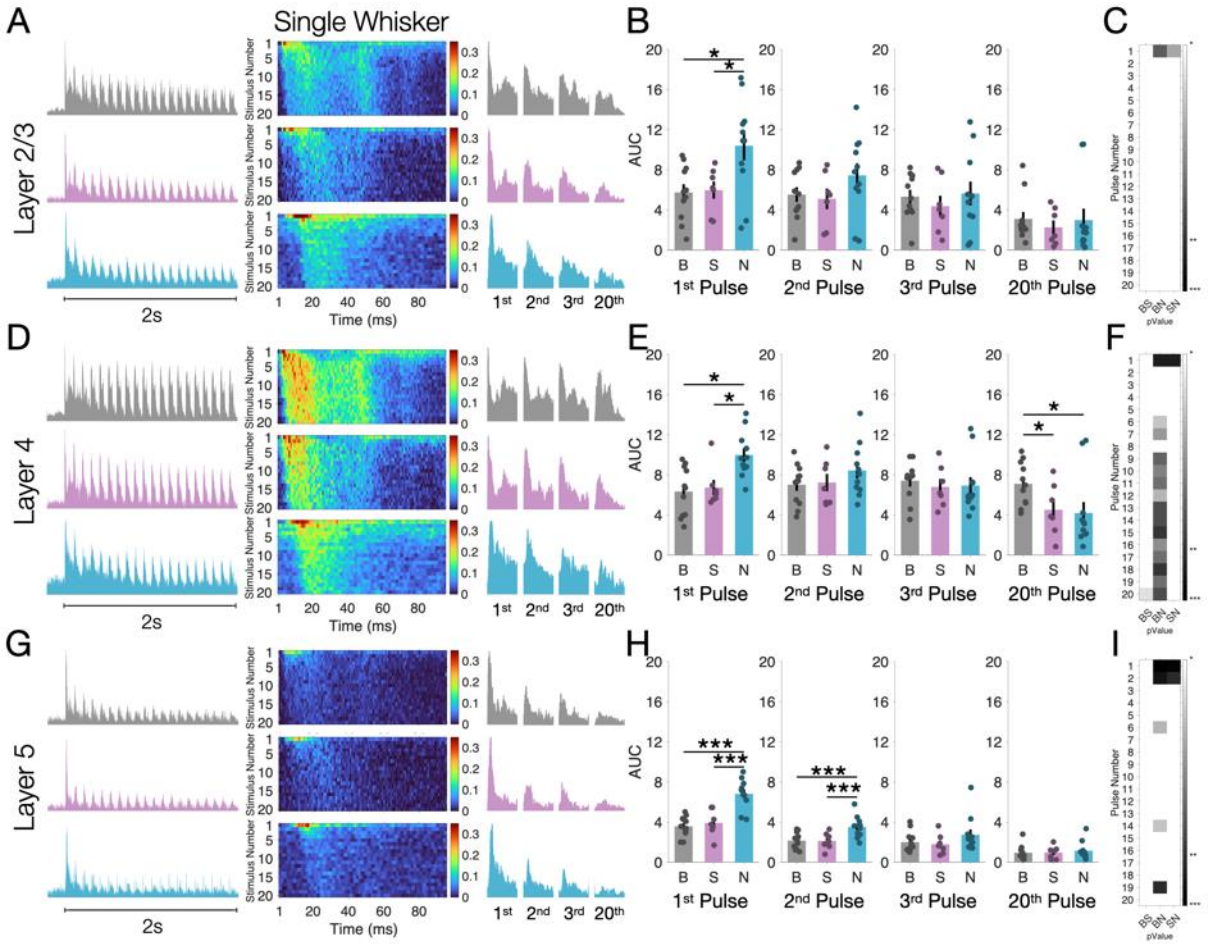

Figure 4, Argunsah et al., 2024

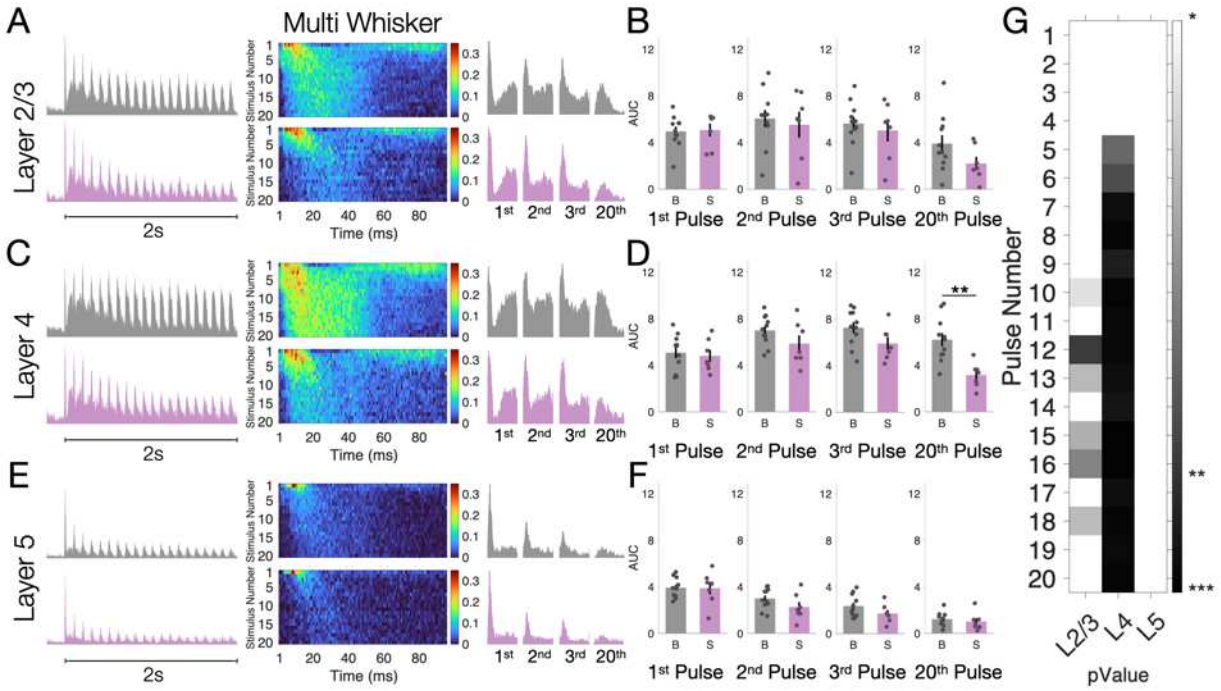

Supplementary Figure 4, Argunsah et al., 2024

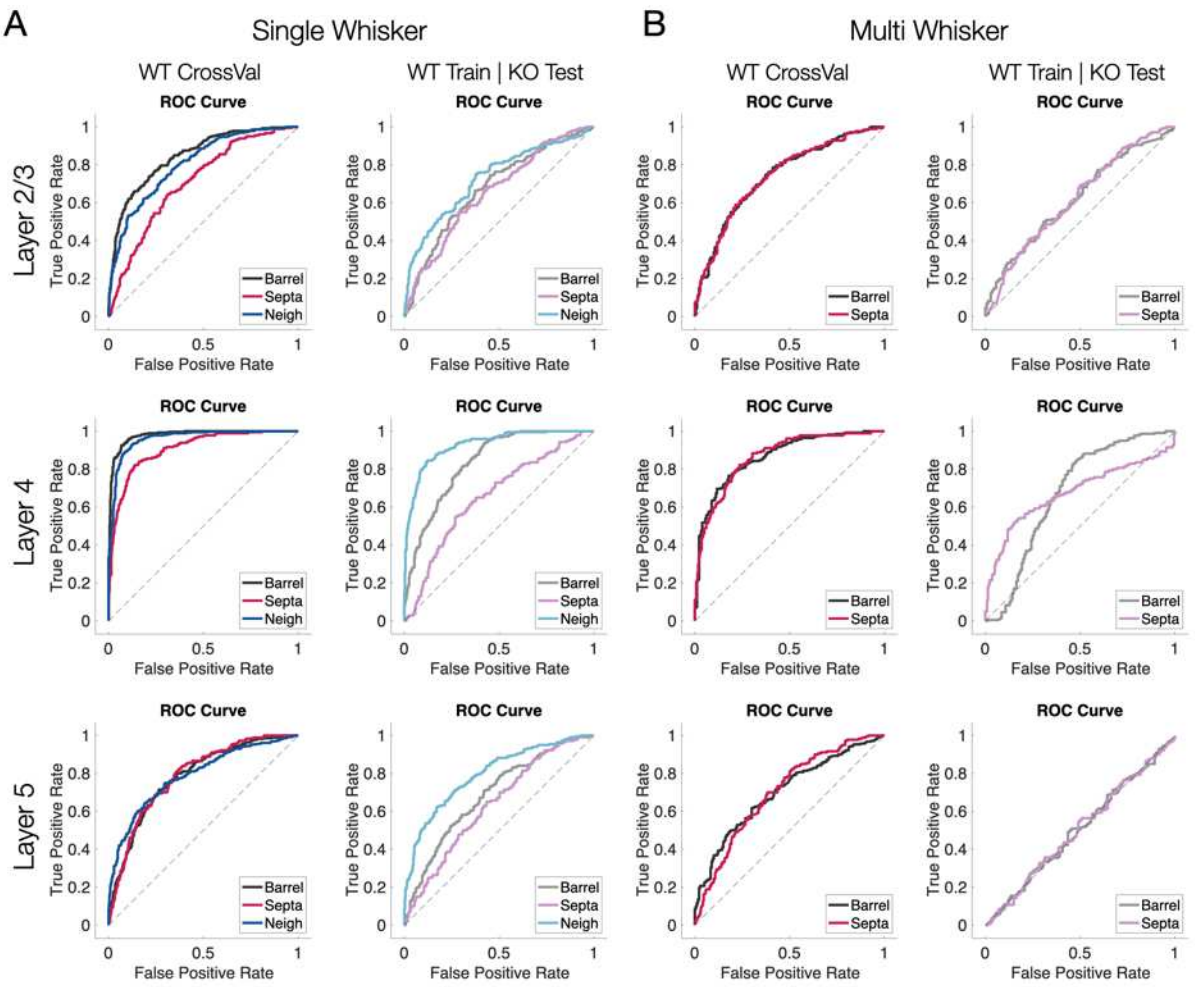

Figure 5, Argunsah et al., 2024

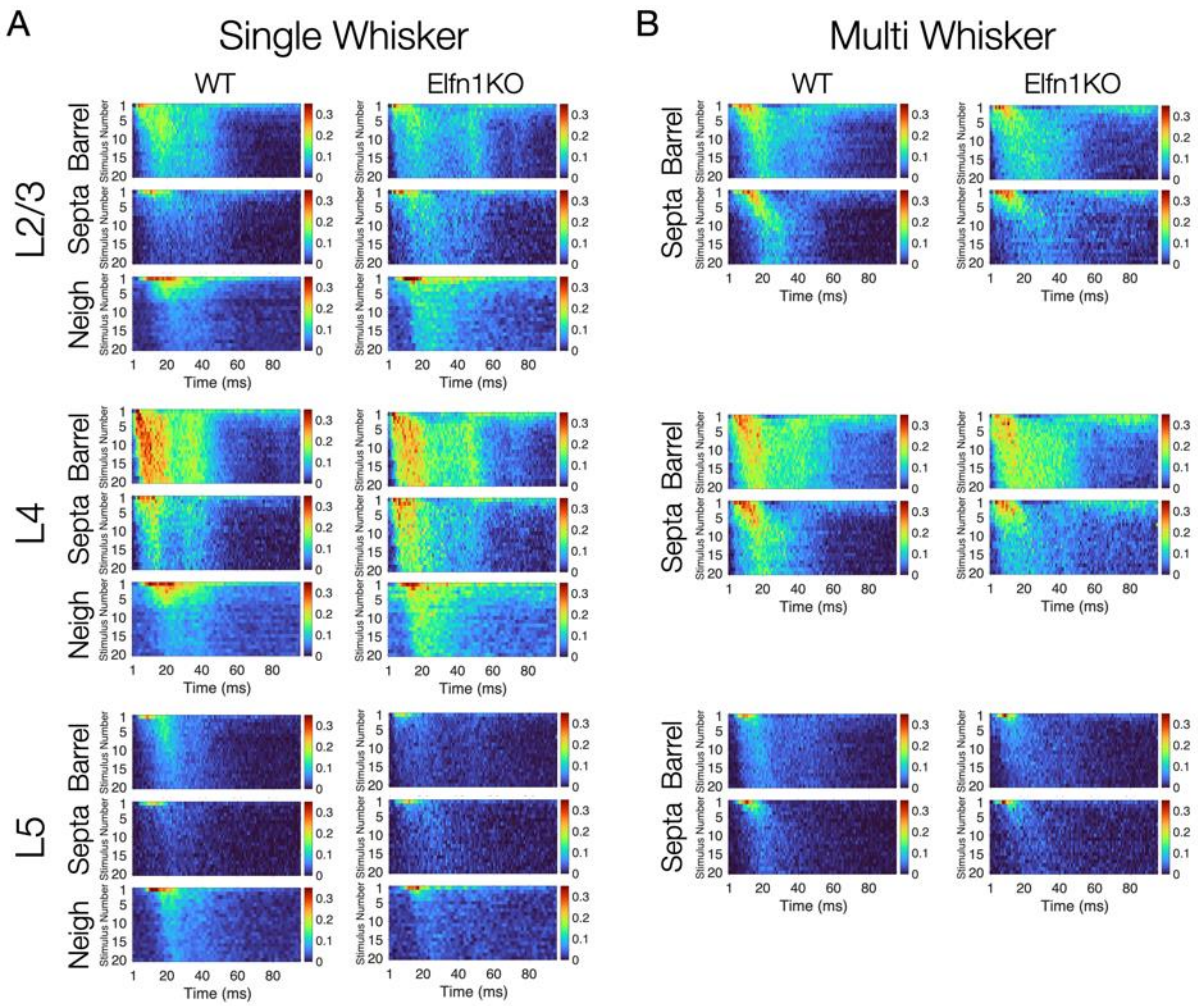

Supplementary Figure 5, Argunsah et al., 2024

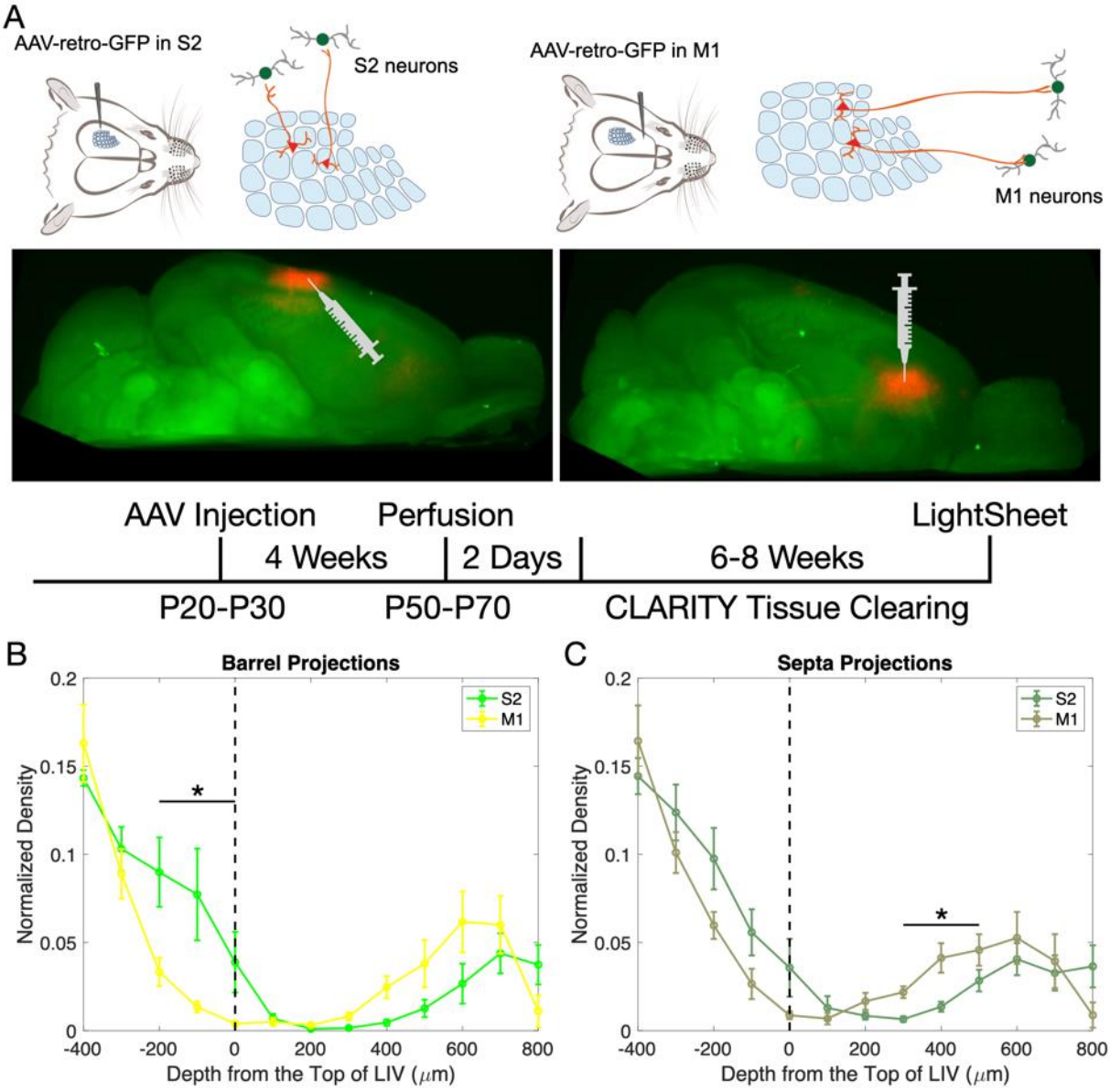

Figure 6, Argunsah et al., 2024